Energy LAB

REVIEW ARTICLE

Energy Lab 2024, 2, 230002

Perovskite/organic tandem solar cells: a review

Yang Ding[1], Hengyue Li[1], Mustafa Haider[1], Yuanji Gao[1], Junliang Yang[1*], Chenyi Yi[2] and Zijian Zheng[3,4,5]

The power conversion efficiency (PCE) of perovskite solar cells (PSCs) has rapidly increased and exceeded 25% based on strategies such as interface modification, doping engineering, and optimization of preparation methods. further improvement seems to have entered a bottleneck period due to Shockley-Quiesser (S-Q) limit of single-junction devices. Tandem cell designed to achieve efficient matching of a wider range of the solar spectrum is considered a successful method to solve this difficulty. In tandem architecture, the PSC is a perfect top-cell candidate owing to its large absorption coefficient, adjustable band gap, and feasible low-temperature solution processibility. The perovskite-based tandem solar cells (TSCs) such as perovskite-silicon, perovskite-perovskite, and perovskite-organic devices have stimulated enormous research interest and got significant progress in the past few years. Among them, the abundant perovskite and organic semiconductor materials with tunable components, adjustable bandgap, and various physical and chemical properties make the perovskite/organic TSCs (PO-TSCs) more competitive. In this work, a general introduction and review of recent advances in perovskite/organic tandem features are provided. In addition, a perspective and some suggestions about future developments in this field are also discussed.

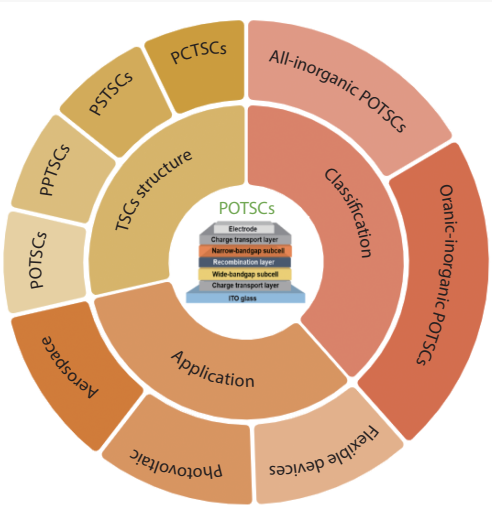

Solar photovoltaics are seen as a potential strategy for addressing future energy and environmental crises. In the past few decades, scientific research on solar cells based on crystalline silicon (c-Si), gallium arsenide (GaAs), copper indium gallium selenide (CIGS), and dye sensitization (DS) has become more and more in-depth and among of them has been widely commercialized. However, there are still some problems that hinder their further large-scale application. Taking crystalline silicon solar cells as an example, the highest efficiency in the laboratory has exceeded 26%, which is very close to the theoretical limit of 29.4% for single junction silicon solar cells[1-5]. Although excellent photoelectric performance, good environmental stability, mature preparation, and packaging technology allow it to achieve commercialization, the prohibitive production cost limits its further expansion of market share. Nowadays, the PCE of solar cells based on perovskite light-absorbing layer with long carrier diffusion length, low defect state density, and large absorption coefficient have reached 25.7% since they were first discovered, which is comparable to that of c-Si solar cells[6-9]. PSCs are favored by researchers and commercial companies and are commonly considered to be a suitable substitute for traditional c-Si solar cells due to their competitive low cost and easy preparation process[10,11]. Nevertheless, no matter what kind of light-absorbing material the solar cells are based on, it is difficult for single-junction devices to achieve efficient use of the solar spectrum. The further improvement of PCE will be restricted by two conditions: thermalization and transmission losses. Transmission losses occur due to the unabsorbed photons with energy less than the bandgap of the materials, while the thermalization loss means that when the energy of absorbed photons is larger than the bandgap, the excess energy will be lost in the form of heat and adversely affect the performance of device[12-17]. To overcome these energy losses and break the S-Q limit, many novel theories such as multijunction solar cells,[18,19] hot-carrier solar cells,[20-21], etc., have been proposed and implemented to improve device efficiency and further reduce manufacturing costs of unit modules. But for now, only tandem solar cells made of multijunction cell structures can meet this demand.

In tandem solar cells, generally, the top sub-cell consists of

[1] *Hunan Key Laboratory for Super-microstructure and Ultrafast Process, School of Physics and Electronics, Central South University, Changsha 410083, China*

[2] *State Key Laboratory of Power System, Department of Electrical Engineering, Tsinghua University, Beijing 100084, China*

[3] *Department of Applied Biology and Chemical Technology, Faculty of Science, The Hong Kong Polytechnic University, Hong Kong 100872, China*

[4] *Research Institute for Intelligent Wearable Systems, The Hong Kong Polytechnic University, Hong Kong 100872, China*

[5] *Research Institute for Smart Energy, The Hong Kong Polytechnic University, Hong Kong 100872, China*

* Corresponding author, E-mail: junliang.yang@csu.edu.cn

Received 31 January 2023; Accepted 28 June 2023; Published online

DOI: 10.54227/elab.20230002

a wide bandgap light-absorbing material to absorb high-energy photons in the solar spectrum, while the bottom cell with a narrow bandgap can absorb the low-energy photons permeated from the top cell. As a result, the incident light is utilized to the greatest extent, achieving a minimized transmission and thermalization loss. Based on this, in theory, double-junction (2J), triple-junction (3J), and infinite-junction tandem devices can achieve the highest PCE of ~46%, ~52%, and ~68% under the illumination of 1 sun (100 mW cm^{-2}, AM1.5G), respectively[22-25]. After successfully achieving a thinner light-absorbing layer film to allow unabsorbed sunlight to pass through, various types of solar cells are assembled into a multi-junction tandem structure to improve the photoelectric performance of the overall device. Theory and research show that the realization of high-performance tandem devices should meet several prerequisites: (1) adjustable wide bandgap to achieve high open-circuit voltage (V_{oc}) and effective absorption of high-energy photons, (2) fewer defects exist in the sub-cell to reduce the carrier recombination in a single cell, (3) high light transmittance of each layer to avoid light loss caused by reflection and scattering as much as possible[26-30]. The high-efficient III-V semiconductors can fulfill these conditions and have been successfully designed into multijunction cells. In recent years, metal halide perovskite solar cells were widely applied to multi-junction tandem solar cells due to their unique features such as tunable wide bandgap in the range from 1.50 to 2.24 eV, fewer defects state density in the film, lower preparation cost, and feasible low-temperature preparation process[31-33].

In perovskite-based TSCs, perovskite devices are often severed as the front sub-cell to absorb high-energy photons in the ultraviolet and visible regions, combined with other lower-bandgap cells to maximally cover the full spectral region from 300 to 1000 nm[34-38]. Many groups have successfully achieved a variety of perovskite-based tandem structures such as perovskite/Si, perovskite/CIGS, perovskite/organic, and perovskite/perovskite with the guidance of theoretical simulation[39-42]. Nevertheless, the cost of monocrystalline silicon and CIGS cells is relatively high due to the expensive raw materials and energy consumption in the production process. As an alternative, perovskite/perovskite TSCs can avoid these restrictions, but several unignorable drawbacks still prohibit their development. Firstly, Sn^{2+} in narrow bandgap perovskite is easily oxidized to Sn^{4+}, thus reducing the stability of the whole device. Secondly, the deposition of narrow bandgap perovskite films will inevitably use high boiling points solvents (such as DMF DMSO), which may penetrate and damage the underlying films and add additional high-temperature annealing process. Compared with narrow bandgap perovskites, organic solar cells (OSCs) with adjustable bandgap can be prepared using low boiling points solvents, giving them unique advantages as a low-bandgap component to combine with perovskite sub-cell for fabricating perovskite-based TSCs. The realization of over 17% higher PCE is owing to the synthesis of new materials, improvement of preparation methods, and the application of ternary or quaternary strategies also suggests a potential future of the commercial application on OSCs[43,44]. Besides, unlike the rigid nature of silicon film, the softness of the films and the feasibility of low-temperature preparation allows PO-TSCs to be assembled on flexible polymer substrates to prepare flexible devices. And it is believed that higher PCE can be obtained than single-junction flexible perovskite and flexible organic solar cell. In addition to achieving complementary absorption of the solar spectrum, the tandem structure can also effectively avoid the damage of ultraviolet light to organic devices and improve the stability of devices, which is another superiority.

Here, we focus on introducing the latest progress of PO-TSCs, related key technologies, and obstacles to the further development. We first concisely introduce the structure and theoretical efficiency limits of TSCs to understand the principles underlying double-junction cells and then we provide an overview of recent progress in PO-TSCs based on all-inorganic perovskite and organic-inorganic hybrid perovskite. The photoelectric performances of varies TSCs are carefully compared to better discuss the limitations of performance improvement. Finally, the potential of PO-TSCs and prospects on the development of stability, large-area fabrication and flexible device are also elaborated.

Structure and theoretical efficiency limit of tandem solar cells

Generally, tandem devices can be divided into two representative structures: two-terminal (2T) monolithically integrated and four-terminal (4T) mechanically stacked TSCs[45-47]. In 2T tandem solar cells, two sub-cells with different bandgaps are connected in optical and electrical series through an intermediate recombination layer (Figure 1a). Therefore, the photocurrent of overall device is limited to the minimum value of two sub-cells while the V_{oc} is the sum of the V_{oc} of two sub-cells subtracting the voltage loss in the tunnel junction[48-52]. In this architecture, the top and bottom sub-cells share a common middle electrode, which is beneficial to reduce the cost of additional transparent electrodes and the light parasitic absorption loss of whole device. Consequently, developing 2T tandem solar cells is an effective strategy to further improve photovoltaic performance and reduce the costs of photovoltaic modules. However, the fabrication process of 2T tandem solar cells is usually complicated, mainly because the top cell is directly deposited on the bottom cell, and its performance is closely related to the quality and morphology of bottom film. The two sub-cells are usually connected by a high-conductivity and transparent intermediate charge recombination layer, which provides recombination sites for electrons and holes extracted from different sub-cells and allows low-energy photons to pass through to the bottom cell with narrow bandgap[53-56]. Compared to 2T tandem solar cells, two complete and independent cells are mechanically stacked together to form 4T tandem structure, in which the front sub-cell needs a transparent electrode as the back electrode (Figure 1a, b)[57]. The photocurrent of two different sub-cells does not need to be matched because each cell works independently only for optical coupling and has no electrical connection, which facilitates to combine with other types of photovoltaic device. For the practical application of 4T TSCs, a necessary transparent electrode remains a crucial issue and a challenge for their further development. At present, the most commonly used transparent

DOI: 10.54227/elab.20230002

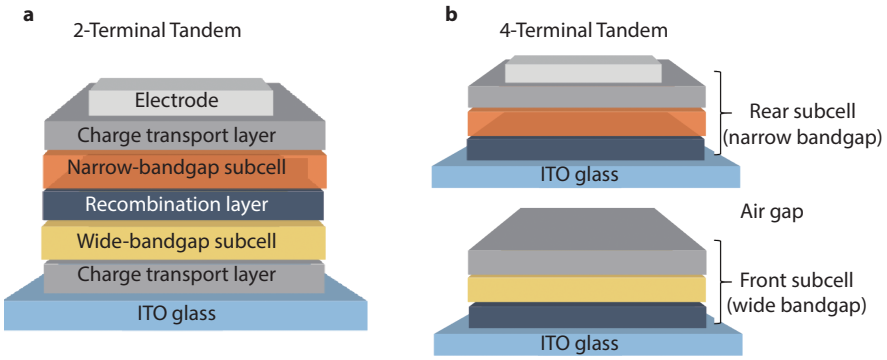

Fig. 1 Schematic diagram of 2T **a** and 4T **b** tandem structure.

electrodes such as indium tin oxide (ITO), indium zinc oxide (IZO), etc. are generally obtained by magnetron sputtering, but the implementation of this technology will cause irreversible damage to the underlying perovskite or organic thin film[58-60]. It is a feasible method to introduce a buffer layer to protect the underlying film or to deposit an ultrathin metal film using thermal evaporation technology as a transparent electrode to replace the metal oxide electrode. Transparent electrodes with a smooth surface tend to cause sunlight transmission loss due to strong light reflection, and the overall manufacturing cost of the device will also increase, which is not conducive to commercial applications. Therefore, the two-terminal (2T) structure has developed rapidly to further decrease costs and obtain excellent photoelectric performances.

According to the S-Q limit, under a standard sunlight intensity, the maximum theoretical PCEs for double-junction TSCs in 2T and 4T configurations can be over 45.7% and 46% respectively, while that of the single-junction solar cell is only ~33%. In single-junction solar cells, only photons with energy greater than the bandgap of photoactive layer can be absorbed and contribute to the photocurrent, while low-energy photons and hot carriers generated by the illumination of light with higher energy will be lost[61-63]. No matter for 2T or 4T TSCs, it is very important to choose light-absorbing layers with suitable bandgap as sub-cells. Since the photocurrent of two sub-cells in the 2T tandem structure needs to be matched, the bandgap of top cell is strictly limited to 1.5-1.9 eV to obtain high PCE, while the sub-cells of 4T structure exist independently of each other, allowing a wider select range of bandgap[64]. But in the perovskite/organic TSCs, the 2T devices have more advantages and challenges than 4T devices. Therefore, the following research progress is mainly about the devices with common 2T tandem structures (Figure 2).

Theoretically, as the key components of a perovskite/organic 2T structure, the properties of wide-bandgap PSC sub-cell, small-bandgap OSC sub-cell, and interconnecting layer (ICL) are critical to the tandem device performance. Because the V_{oc} of TSCs should be the sum of V_{oc} of each sub-cell, high V_{oc} loss of each sub-cell is detrimental to the device efficiency. Moreover, ICL, which determines the final fill factor (FF), V_{oc}, and J_{sc} values, also plays an important role in balancing photovoltaic parameters. After optimizing the performance of each sub-cell and carefully designing ICL, based on the current optimal photovoltaic parameters that have been realized in perovskite and organic solar cell systems, the PCE of perovskite/organic TSCs can reach more than 31%[65-70]. Therefore, perovskite/organic tandem structure will exhibit more practical applications with the advantages of high theoretical limit efficiency and solution processability.

Perovskite/organic tandem solar cells

In recent years, PSCs have attracted much attention as an ideal light-absorbing material in solar cells, but the further improvement of their PCE has entered a bottleneck period and it is difficult to make a greater breakthrough. Taking advantage of the adjustable bandgap characteristics of perovskite materials to fabricate perovskite-based tandem solar cells is considered to be an effective strategy to break through the PCE limit of single-junction solar cells[71-73]. Under actual conditions, obtaining a tandem structure by continuous deposition methods without damaging the underlying films is a key challenge for preparing perovskite-based tandem solar cells. Same as the perovskite photoactive layer, organic photovoltaic solar cells also have feasible solution processability, and provide unique advantages in the preparation of flexible and large-area devices. In addition, tin-based PSCs with narrow bandgap have poor stability in the air due to the Sn^{2+} in the precursor solution that is easily oxidized to Sn^{4+}, which is not conducive to the practical application of perovskite/perovskite TSCs. Narrow bandgap organic solar cells have better stability and absorption tunability, making them the most excellent alternative for the bottom sub-cell in the perovskite-based tandem structure[74]. Moreover, it is not a good choice to fabricate an all-organic tandem device because the wide bandgap organic bulk heterojunction (BHJ) as the front sub-cell will cause serious open circuit voltage loss to the whole devices. In contrast, the large bandgap PSCs have lower energy losses and higher absorption intensity in the visible light range, which makes the PO-TSCs a better integration [75]. As the front sub-cell in tandem structure, the different components of wide bandgap perovskite and their intrinsic characteristics are very important for the performance of whole tandem device. Figure 3 illustrates the PCE evolution of single-junction OSCs, single-junction PSCs, PO-TSCs based all-inorganic perovskite and perovskite/organic tandem solar cells based organic-inorganic hybrid perovskite sub-cells. In recent years, the highest PCE of PO-TSCs (24.00%) has far exceeded that of a single-junction OSC and is close to that of a

DOI: 10.54227/elab.20230002

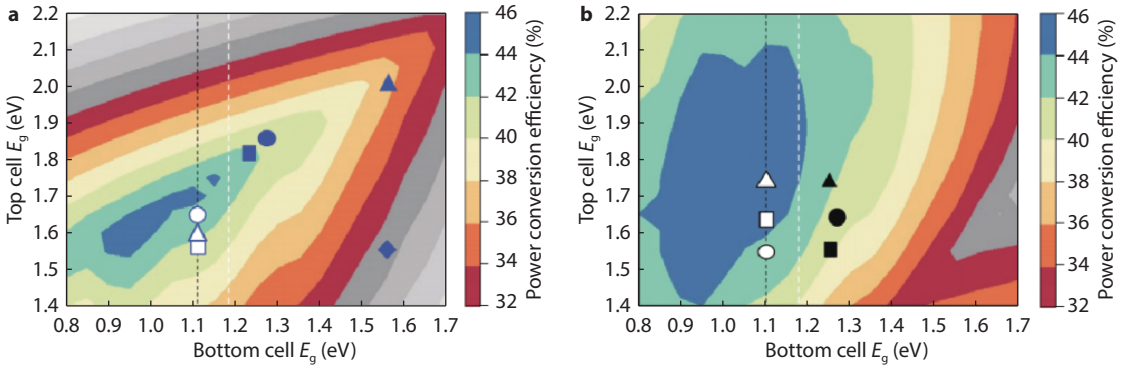

Fig. 2 Theoretical PCEs for 2T and 4T TSCs[64]. Copyright 2023, Springer Nature.

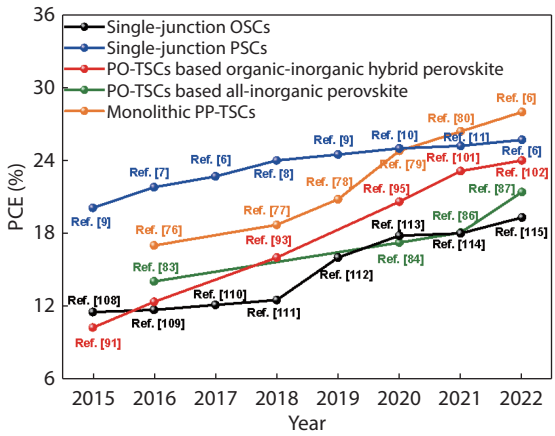

Fig. 3 The PCE evolution of single-junction OSCs, single-junction PSCs, PO-TSCs based all-inorganic perovskite, perovskite/organic tandem solar cells based organic-inorganic hybrid perovskite sub-cells and monolithic all-perovskite tandem devices.

single-junction PSC, demonstrating outstanding research value and potential. In order to better understand the photoelectric performance of PO-TSCs and determine the factors that prevent them, we systematically compare the performance parameters of all-perovskite tandem solar cells (PP-TSCs) and PO-TSCs[76-80]. From the perspective of the device structure, narrow bandgap sub-cell cause differences in the overall performance of perovskite-based TSCs. The highest PCE of PP-TSCs has reached a remarkable 28% while that of PO-TSCs is around 24% now[6,102]. It should be noted that the J_{sc} of champion PO-TSCs is far lower than that of champion PP-TSCs, which is the most obvious discrepancy in photovoltaic parameters. Other device parameters such as FF and V_{oc} have little differences and all display high values. The main reason is that perovskite/organic tandem devices exhibit lower photocurrent conversion potential, leading to a lower J_{sc} value of OSC sub-cell. Overall, the slightly lower photoelectric performance of PO-TSC is mainly limited by its narrow band gap OSC sub-cell, which can be further improved by optimizing the wide-bandgap perovskite sub-cell. Therefore, the following will introduce the related progress of perovskite/organic TSCs around different perovskite components with wide bandgap (all inorganic and organic-inorganic hybrid perovskite, respectively).

All-inorganic perovskite and organic tandem solar cells

All-inorganic perovskite solar cells have unique advantages in the practical application of PSCs due to their competitive environmental stability and achieved rapid development in recent years. Performance, bandgap and interconnecting layer information of all-inorganic perovskite and organic TSCs are shown in Table 1. However, the PCE of all-inorganic PSCs cannot catch up with that of the organic-inorganic hybrid devices limited to narrow absorption bands. Among the all-inorganic materials, $CsPbI_2Br$ which features a moderate thermal transition temperature and good thermal stability was widely employed in PSCs[81-83]. Besides, $CsPbI_2Br$ with a bandgap of 1.92 eV PSCs can achieve a high external quantum efficiency (EQE) near 90% within 350-615 nm, proving that $CsPbI_2Br$ is suitable for serving as a short-wavelength sunlight absorber for TSCs. In 2020, Lang et al. developed all-inorganic perovskite/organic TSCs with $CsPbI_2Br$ and PTB7-Th:IEICO-4F active layers (Figure 4a), which can form a good complementary absorption of sunlight with a wavelength from 300 to 1000 nm[84]. P3HT/MoO_3/Ag/PFN-Br was adopted as the ICL to join the front and rear sub-cells. As shown in Figure 4b, the front sub-cell can absorb most high-energy photons and obtain a maximum EQE value of 89% at 440 nm, while the rear cell exhibits higher EQE values in the near infrared region (650 nm-1000 nm) rather than the visible light region. The perovskite-based front sub-cell and ICL perform transmission of over 70% in the near-infrared region, which allows enough sunlight to pass through and reach the underlying cell. After optimizing the thickness of PTB7-Th:IEICO-4F active layers, the J_{sc} of front and rear sub-cells reached a good balance. A remarkable high PCE of 17.24% was achieved, which was significantly higher than that of the single-junction solar cells (Figure 4c). The research indicates that the TSCs combining all-inorganic perovskite and narrow bandgap organic solar cells is a feasible strategy to realize full utilization of a broad solar spectrum and high PCE.

In the same year, Jang's research group selected the same perovskite and organic materials as the front and back sub-cell to fabricate perovskite-organic tandem devices and increased the PCE to 18.04% successfully[85] (Figure 4d). Moreover, attributing to the hydrophobicity of the PTB7-Th:IEICO-4F back cell, the long-term stability of perovskite devices under humid conditions was also enhanced in hybrid TSCs. To further explore the promise in the field of inorganic

DOI: 10.54227/elab.20230002

Table 1. Performance summary of all-inorganic perovskite and organic TSCs.

Perovskite/organic absorbers	Bandgap (eV)	ICL	V_{oc} (V)	J_{sc} (mA cm^{-2})	FF (%)	PCE (%)	Ref.
$CsPbI_2Br$/PTB7Th:COi8DFIC:$PC_{71}BM$	/	MoO_3/Au/ZnO	1.71	11.98	73.40	15.04	[83]
$CsPbI_2Br$/PTB7Th:IEICO-4F	1.92/1.20	MoO_3/Ag/PFN-Br	1.82	13.20	71.68	17.24	[84]
$CsPbI_2Br$/PTB7-Th:IEICO-4F	1.85/1.25	MoO_x/Au/ZnO	1.73	12.94	81.00	18.04	[85]
$CsPbI_{2.1}Br_{0.9}$/PM6:Y6	1.79/1.30	MoO_3/Ag/ZnO	1.89	12.77	74.81	18.06	[86]
$CsPbI_2Br$/PM6:Y6	1.92/1.40	MoO_3/Ag/PFN-Br	2.22	12.68	76.00	21.40	[87]
$CsPbBr_3$/PBDB-T-SF:IT-4F (4T)	2.30/1.29	/	/	/	/	14.03	[88]
$CsPbI_2Br$/PM6:Y6	1.90/1.33	MoO_3/Au/ZnO	1.95	12.46	75.59	18.38	[106]
$CsPbI_{2.25}Br_{0.75}$/D18-Cl-B:N3:$PC_{61}BM$ (4T)	/	/	/	/	/	22.34	[89]
$CsPbI_2Br$/PM6:CH1007	1.90/1.30	/MoO_3/Au/ZnO	2.10	14.23	77.70	23.21	[90]

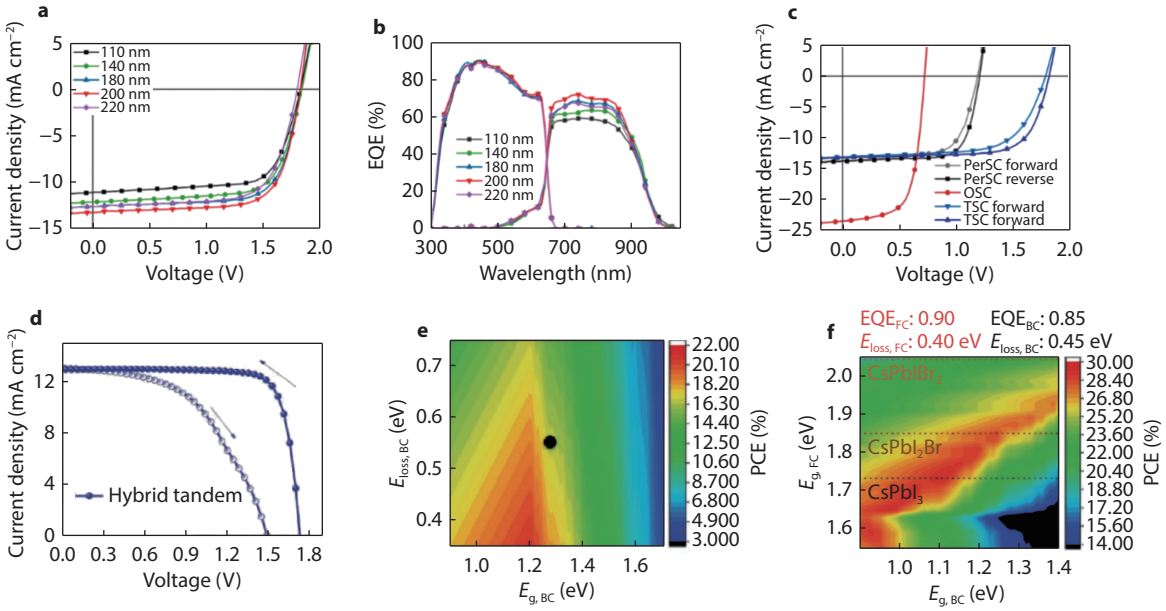

Fig. 4 **a** *J-V* and **b** EQE curves of TSCs with different thicknesses of the organic active layer; **c** *J-V* curves of the best-performance single-junction PSC, OSC, and TSC[84]. Copyright 2020, American Chemical Society. **d** *J-V* characteristic of the hybrid tandem device under AM 1.5G one-sun illumination[85]. Copyright 2020, John Wiley and Sons. **e** Semi-empirical calculation of the PCE of hybrid tandem devices with respect to $E_{loss,\ BC}$ and $E_{g,\ BC}$. **f** Semi-empirical calculation of the PCE of hybrid tandem devices with respect to $E_{g,\ FC}$ and $E_{g,\ BC}$ when using the best-reported parameters of sub-cells[85]. Copyright 2020, John Wiley and Sons.

perovskite/organic hybrid devices, a semi-empirical analysis was conducted to determine strategies for further improvement. Figure 4e and 4f show the calculation PCE of tandem devices based on the optimization of EQE, E_{loss} and E_g of the back and front cells (marked as EQE_{BC}, $E_{loss,BC}$, $E_{g,BC}$ and $E_{g,FC}$, respectively). According to the calculation results, a high 28.27% PCE of TSCs can be achieved with the $CsPbI_2Br$ (1.85 eV) front cell, which is a promising result comparable to that of state-of-the-art perovskite/Si tandem devices and shows greater competitiveness as a new photovoltaic technology for industrialization.

More recently, as can be seen in the absorption spectra displayed in Figure 5a, Xie's research group also reached a similar conclusion by characterizing the UV visible spectrum of the thin films. The perovskite thin films show a very strong absorption among visible light region with absorption peaked at ~450 nm, and the corresponding cell also exhibits a high EQE value in the entire visible light region, which compensates for the relatively low EQE in OSCs. A high-performance monolithic perovskite/organic TSCs based on the integration of $CsPbI_2Br$ PSC with a PM6:Y6-based or PTB7-Th:O6T-4F-based bulk-heterojunction OSC was demonstrated, and a higher PCE of 18.38% was obtained using PM6:Y6 organic material as rear sub-cell (Figure 5b). Using the same PM6:Y6 as the organic light-absorbing layer, Zhu's research group optimized the composition of the all-inorganic perovskite ($CsPbI_{2.1}Br_{0.9}$) to prepare TSCs. The *J-V* curves of the champion tandem device and sub-cells are shown in Figure 5d. The champion efficiency of single junction OSCs is 14.01%, while the prepared champion perovskite/organic series device has a PCE of 18.06%, a V_{oc} of 1.89 V, a J_{sc} of 12.77 mA cm^{-2}, and FF of 74.81%. It is worth noting that the performance of the device remains unchanged no matter after 150 h of UV irradiation, 250 h under one sun illumination, or 100 h of heating at 80 °C, respectively, showing excellent long-term stability under harsh environmental conditions compared with the organic-inorganic hybrid perovskite-based TSCs (Figure 5e)[86]. The long-term service life of photovoltaic products is usually considered as one of the most important evaluation indicators. As depicted in Figure 5f, in a tandem structure, ultraviolet light is mostly absorbed by the front perovskite cell, protecting the OSC bottom cell from ultraviolet radiation. Con-

DOI: 10.54227/elab.20230002

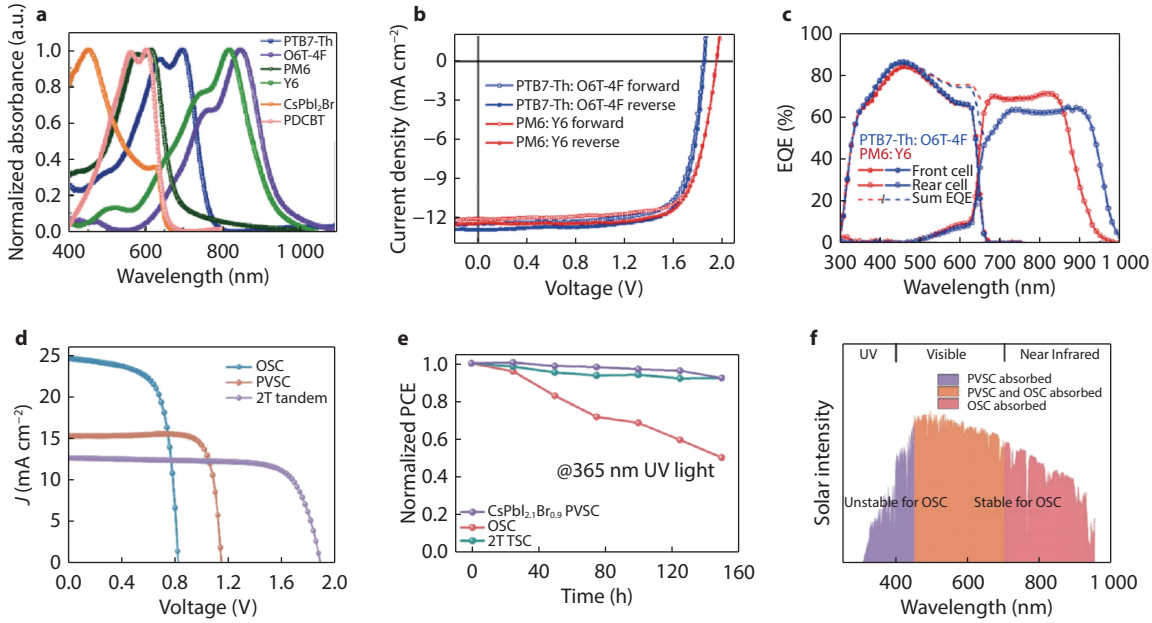

Fig. 5 **a** Absorption spectra of the different materials used in the tandem cell. **b** *J-V* curves of tandems cells, measured under AM1.5G simulated illumination. **c** EQE spectra of the corresponding tandem cells[107]. Copyright 2020, Elsevier. **d** The *J–V* curves of the single junction wide-bandgap PVSC, single-junction narrow-bandgap OSC, and 2T tandem solar cell under AM 1.5G illumination. **e** PCE evolution of the single-junction $CsPbI_{2.1}Br_{0.9}$ PVSC, OSC and 2T tandem solar cells under 365 nm UV light. **f** Schematic illustration of the filtering of UV light by the perovskite top cell to protect the UV-unstable OSCs[86]. Copyright 2021, Royal Society of Chemistry.

versely, on the other hand, building TSCs with all-inorganic perovskite not only improves their stability, but also is considered a promising strategy to break the efficiency bottleneck of 20% for OSCs. By inserting the s-ZnO layer in the perovskite sub-cell and employing thermal annealing (TA)-free process in the fabrication of the rear sub-cell, Gu. et al achieved a remarkable PCE of 20.6% with a record high V_{oc} of 2.116 V in monolithic 2T-TSCs configuration. In the same year, using a dopant-free low-cost polymer PTQ10 as a hole transport layer (HTL) for $CsPbI_2Br$ PSC, Ding et al got a champion PCE of 17.8% with a high V_{oc} of 1.4 V. Meanwhile, the ICL employing PTQ10 HTL also exhibits excellent optical and electrical properties for the application in monolithic $CsPbI_2Br$/PM6:Y6 TSC. As a result, TSCs present the highest PCE of 21.4 % (21.3%), with the record high V_{oc} of 2.22 V[87]. This work shows the excellent performance of PTQ10 as HTL and demonstrates that the development of efficient HTL is essential to further improve the performance of PSCs and TSCs. As we all know, the performance of OSCs will rapidly decay under conditions of continuous ultraviolet radiation because of their intrinsic chemical instability characteristics. In addition to conventional $CsPbI_2Br$, some research groups also tried to choose other all inorganic perovskite. Li's group constructed an inorganic-perovskite/organic 4T TSC based on a semitransparent inorganic $CsPbBr_3$ PSC (Figure 6a) to address the tricky stability issues of single-junction OSCs[88]. The high-quality $CsPbBr_3$ photoactive film was prepared with a dual-source vacuum co-evaporation method, using stoichiometric precursors of CsBr and $PbBr_2$ under a low evaporation rate. The top inorganic $CsPbBr_3$ perovskite solar cells not only contribute to the performance of whole device, but also act as a UV filter to ameliorate environmental stability. The *J-V* curves and EQE spectra of the semitransparent PSCs and the filtered bottom OSCs are shown in Figure 6b and 6c. The final perovskite/organic TSCs obtained a PCE of 14.03% and also held excellent long-term stability under UV-light irradiation. Although 2T tandem solar cells are more popular because of their higher PCE, for 4T tandem cells, the two sub-cells are obtained separately without complex equipment to produce high-quality interconnecting layers. In addition, the photoelectric performance of 4T structure devices is less sensitive as the spectrum changes. In 2023, Ding's group made 4T inorganic perovskite/organic tandem solar cells by using semi-transparent inorganic PSC and D18-Cl-B:N3:PC_{61}BM OSC as the sub-cells and obtained a PCE of 21.25%. They also made equivalent 2T tandem cells by connecting the champion semi-transparent PSC and OSC in series. The best single-junction OSC shows a PCE of 18.17% and the semi-transparent $CsPbI_2Br$ solar cells exhibits a PCE of 12.99% (Figure 6d and 6e). Using different interconnecting layers of HTL/MoO_3/ITO/Ag/PDIN and PEDOT:PSS/ITO/SnO_2/ZnO for the tandem cells, 2T series devices got high PCEs of 19.18% and 18.83%, respectively. After that, they developed a modified drop-coating method to prepare PSCs, which show better photovoltaic performances than the spin-coated films. To make 4T tandem cells, the semi-transparent PSC was put onto the OSC to maximize the PCE of the filtered OSC, which yields a best PCE of 8.26% (Figure 6f and 6g). The PCE of 4T TSC using $CsPbI_{2.25}Br_{0.75}$ and D18-Cl-B:N3:PC_{61}BM sub-cells was improved to 22.34%, which is one of the highest PCE of the reported 2T and 4T PO-TSCs [89]. A large number of defects at the interface of the wide-bandgap sub-cell in the all-inorganic perovskite/organic tandem structure are the key factors that restrict the overall performance of the tandem device. In the same year, Xie's group pointed out a dual-interface engineering approach to modify the bottom and top interfaces of wide-bandgap $CsPbI_2Br$ films[90]. As a result,

DOI: 10.54227/elab.20230002

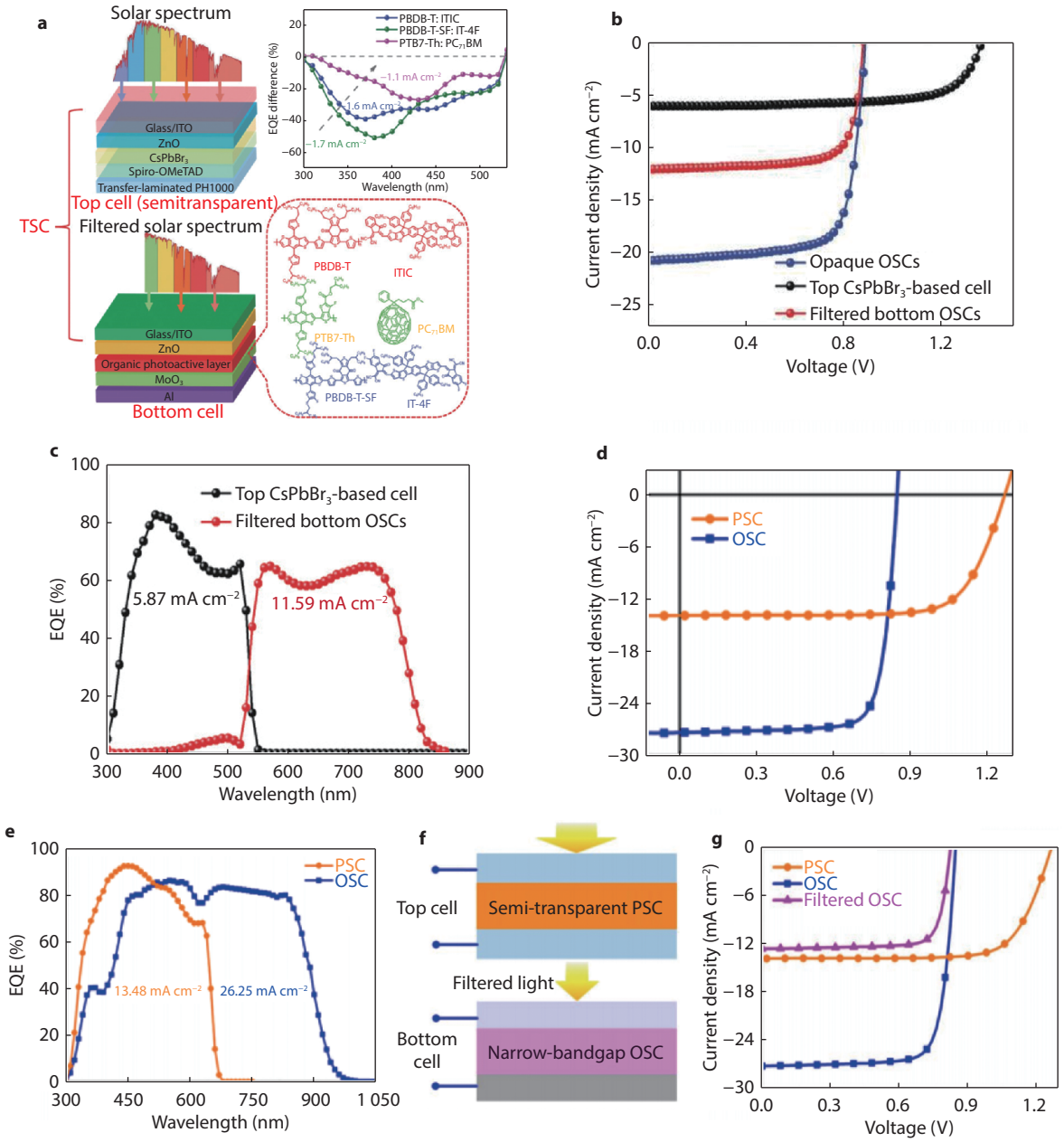

Fig. 6 **a** Device structure of 4T TSCs: semitransparent top cell with a structure of glass/ITO/ZnO/$CsPbBr_3$/spiro-OMeTAD/transfer-laminated PH1000; bottom OSCs with a structure of glass/ITO/ZnO/organic photoactive layer/MoO_3/Al, and molecular structures of donor and acceptor materials used in the corresponding organic photoactive layer. **b** *J-V* curves of the top semitransparent $CsPbBr_3$-based solar cell illuminated from the glass/ITO side, and the small-bandgap PBDB-T-SF:IT-4F-based bottom OSC with and without the $CsPbBr_3$-based semitransparent device functioning as a filter. **c** EQE spectra of a $CsPbBr_3$-based top semitransparent solar cell and a filtered PBDB-T-SF:IT-4F-based bottom OSC[93]. Copyright 2018, John Wiley and Sons. **d** *J-V* curves for the semi-transparent $CsPbI_2Br$ solar cells and organic solar cells. **e** EQE spectra for the semi-transparent $CsPbI_2Br$ solar cells and organic solar cells. **f** Structure for the 4-terminal perovskite/organic tandem solar cells. **g** *J-V* curves for the best semi-transparent PSC (top cell), stand-alone OSC, and filtered OSC (bottom cell)[89]. Copyright 2022, Springer Nature.

$CsPbI_2Br$ with uniform and fully covered surface morphology, large-size grain, and remarkably passivated interfacial defects are prepared. After optimization, the wide-bandgap $CsPbI_2Br$ sub-cell generated a high PCE of 17.0% and V_{oc} of 1.347 V. By integrating it with a narrow-bandgap PM6:CH1007 sub-cell, tandem device shows a new record PCE of 23.21% and exhibits good long-term stability due to the improved $CsPbI_2Br$ films. Defect passivation has been proven to be one of the effective strategies for improving device performances.

Organic-inorganic hybrid perovskite and organic tandem solar cells

Compared with all inorganic perovskite, organic-inorganic hybrid perovskite sub-cells has more advantages in PCE. Information on device structure and performance are summarized in Table 2. For 2T perovskite/organic TSCs, the surface morphology and film quality of the perovskite light-absorb-

DOI: 10.54227/elab.20230002

Table 2. Performance summary of organic-inorganic hybrid perovskite and organic TSCs.

Perovskite/organic absorbers	Bandgap (eV)	ICL	V_{oc} (V)	J_{sc} (mA cm^{-2})	FF (%)	PCE(%)	Ref.
$MAPbI_3$/PBSeDTEG8:PCBM	1.57/1.28	PEDOT:PSS PH500/PEDOT:PSS4083	1.52	10.05	67.00	10.23	[91]
$MAPbICl_2$/PBDTT-DPP:$PC_{70}BM$	1.63/1.25	PFN/doped-MoO_3/MoO_3	1.58	8.02	68.00	8.62	[92]
$MAPbI_3$/PCE-10:$PC_{71}BM$	1.57/1.33	C_{60}-SB/Ag/MoO_3	1.63	13.10	75.10	16.00	[93]
$FA_{0.8}MA_{0.02}Cs_{0.18}PbI_{1.8}Br_{1.2}$/PBDBT-2F:Y6:$PC_{71}BM$	1.77/1.41	BCP/Ag/MoO_x	1.90	13.05	83.10	20.60	[95]
$MAPbI_{2.95}Cl_{0.05}$/PM6:Y6	1.58/1.40	C_{60}-ionene/Ag/MoO_3	1.92	12.60	79.00	19.20	[97]
$MA_{0.96}FA_{0.1}PbI_2Br(SCN)_{0.12}$/PM6:CH1007	1.72/1.30	PCBM/BCP/Au/MoO_3	1.96	13.80	78.40	21.20	[98]
$FA_{0.6}MA_{0.4}Pb(I_{0.6}Br_{0.4})_3$/PTB7-Th:BTPV-4Cl-eC9	1.78/1.22	C_{60}/BCP/Ag/MoO_x	1.88	15.70	74.60	22.00	[100]
$MA_{1.06}PbI_2Br(SCN)_{0.12}$/PM6:Y6	1.70/1.40	PCBM/BCP/Au/MoO_3	1.93	14.30	72.50	20.03	[99]
$Cs_{0.25}FA_{0.75}Pb(I_{0.6}Br_{0.4})_3$/PM6:Y6	1.79/1.36	C_{60}/BCP/CRL/MoO_x	2.06	14.87	77.00	23.60	[101]
$FA_{0.8}Cs_{0.2}Pb(I_{0.5}Br_{0.5})_3$/PM6:Y6	1.85/1.40	SnO_x/InO_x /MoO_x	2.15	14.00	80.00	24.00	[102]
$Cs_{0.1}(FA_{0.6}MA_{0.4})_{0.9}Pb(I_{0.6}Br_{0.4})_3$/PBDB-T:SN6IC-4F	1.74/1.30	Ag/PEDOT:PSS	1.85	11.52	70.98	15.13	[103]

ing layer or the selection of the interconnecting layer is critical to the photoelectric performance of overall device. As early as 2015, Yang and co-workers selected PBSeDTEG8 with photosensitivity up to 950 nm to broaden the photo-response and successfully achieved a high PCE of 10.23% for tandem solar devices[91]. In 2016, Liu et al. designed a nanostructured perovskite film and select a PFN/doped MoO_3/MoO_3 structure as the interconnecting layer (ICL) to prepare the 2T PO-TSC[92]. Thanks to this nanostructure, the PCBM layer can be fully filled to obtain a close contact interface with the perovskite layer, which can not only facilitate the extraction and transport of carriers at the interface, but also could alleviate the hysteresis effect of device. The doped MoO_3 interconnect layer provides efficient recombination sites for electrons and holes generated from the front and back sub-cells, and protects the underlying film from damage during continuous solution deposition. Based on these strategies, the PO-TSC with the structure shown in Figure 7a achieved 8.62% PCE with a high V_{oc} of 1.58 V and FF of 0.68 (Figure 7b). The result indicated the effectiveness of the doped-ICL in promoting carriers to recombine with a lower energy loss and provided a potential development strategy for high-performance tandem devices. According to the research, Liu et al. pointed out a fact that if the perovskite was set as the front sub-cell in perovskite/polymer TSCs, the thick perovskite active layer (about hundreds of nanometers) would severely hinder the sunlight from reaching the back sub-cell. To solve this problem, a new strategy that combined a thin perovskite layer with organic polymer was implemented to enhance light absorption and boost PCE. They integrated a ~90 nm thick perovskite top sub-cell and a ~100 nm thick polymer: fullerene blend bottom sub-cell through a graded intermediate recombination layer consisting of a zwitterionic fullerene, silver (Ag), and molybdenum trioxide (MoO_3). The perovskite/polymer TSC with the architecture of ITO/PEDOT:PSS/Perovskite/$PC_{61}BM$/C_{60}-SB/Ag/MoO_3/PolymerBHJ/ C_{60}-N/Ag (Figure 7c) achieved a record PCE of 16.0% with poor hysteresis, which is 75% higher than the single junction PSCs (Figure 7d) [93]. Additionally, the

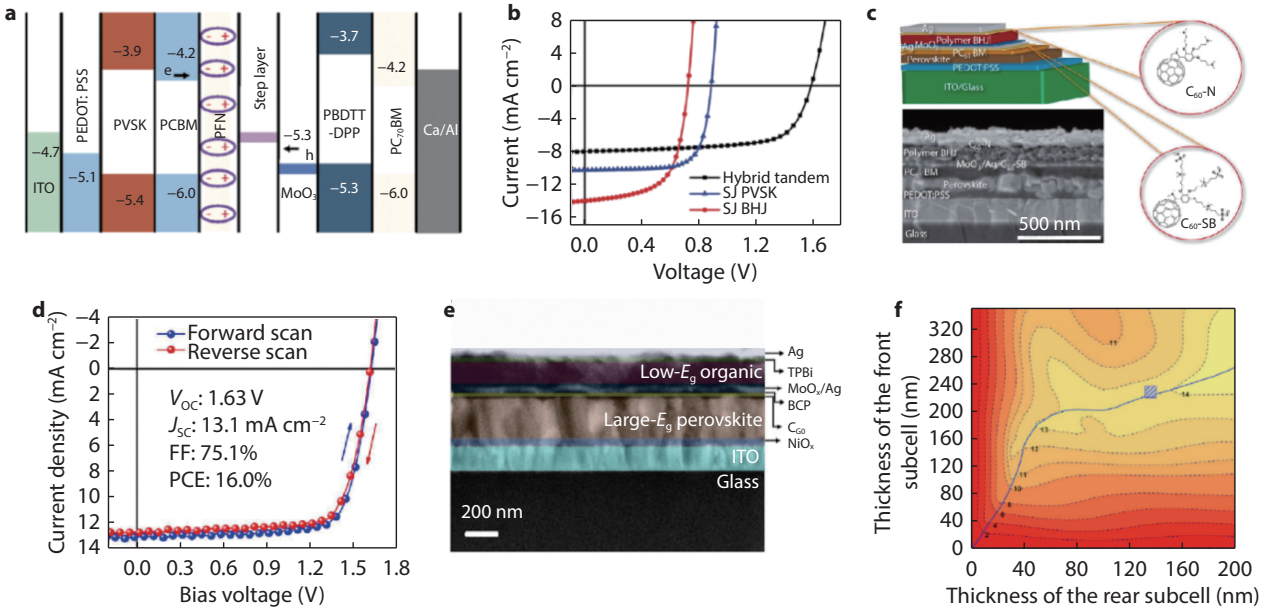

Fig. 7 **a** Device architecture with corresponding energy levels for the hybrid TSC. **b** *J-V* characteristics of single-junction PVSK and PBDTT-DPP:$PC_{70}BM$ reference solar cells and hybrid tandem solar cell[88]. Copyright 2016, Royal Society of Chemistry. **c** Device structure and cross-sectional SEM image of a tandem device with a perovskite layer thickness of ~90 nm. **d** *J-V* curves and device metrics of the optimal polymer/perovskite hybrid TSC[92]. Copyright 2016, American Chemical Society. **e** Cross-section SEM of PO-TSC. **f** Stimulated current density as a function of the variable thicknesses of the front and rear sub-cells[95]. Copyright 2020, Elsevier.

DOI: 10.54227/elab.20230002

adopted methodology provides an alternative to substantially reduce the amount of toxic lead in the device, while still maintaining high performance.

In tandem structure, the perovskite possesses smaller voltage loss (E_{loss}) and higher external quantum efficiency (EQE) response compared with the organic counterparts while low bandgap organic solar cells offer potentially better stability and absorption tunability than their narrow bandgap Sn-based perovskite counterparts[94]. After theoretical analysis, the potential PCE of the perovskite/organic tandem cells shows a maximum calculated value of over 31% when the bandgaps of the sub-cells are well optimized, which provides useful theoretical and experimental guidance for the fabrication of all-solution processed tandem cells. Taking both model analysis and the realistic performance levels of photovoltaic devices into consideration, Yang and co-workers select a combination of PBDBT-2F:Y6:$PC_{71}BM$ organic solar materials with an E_g of 1.41 eV as the bottom cell and $FA_{0.8}MA_{0.02}Cs_{0.18}PbI_{1.8}Br_{1.2}$ of suitable 1.77 eV band gap as the absorber of the top cell, and obtain an iconic high PCE over 20%[95]. The thickness of the absorption layer of the two sub-cells has an important influence on the light absorption intensity and PCE of the overall device. Figure 7e and 7f show the cross-section SEM of TSCs and the relationship between the photo-current and the thickness of each sub-cell, respectively. The position on the highlighted blue curve indicates that the current is theoretically matched, providing a valuable reference for optimizing the thickness of the photoactive layer to meet the current effectively. In addition to the type and thickness of sub-cells, the selection and thickness of the interconnecting layer also seriously affect the overall performance of the tandem device, which is required to simultaneously fulfill the high electrical, optical, and chemical requirements[96].

Recently, after optimizing the thickness of perovskite film, Zhang's group developed a thickness-insensitive and solvent-resistant interconnecting layer to efficiently connect perovskite and organic sub-cells with low contact resistance. As shown in Figure 8a and 8b, perovskite thin films with various thicknesses show different visible spectral transmittance and short circuit current densities of devices. And the resultant perovskite-organic tandem devices maintain high efficiencies over a wide thickness range of interconnecting layer, from ~20 nm to ~50 nm, providing an easily fabricated, solvent-resistant platform to integrate perovskite and organic active layers with low-temperature solution processing techniques. Finally, the tandem device with a structure of $MAPbI_{2.95}Cl_{0.05}$/PM6:Y6 give a maximum efficiency of 19.2% and highly reproducible 1 cm^2 tandem devices also realized a high PCE of 17.8%, which bespeaks great significance in design of ultrathin and facile solution-processed PO-TSCs (Figure 8c)[97].

Although the facile solution fabrication process gives the perovskite/organic tandem solar cells extremely advantageous, the lack of wide-bandgap perovskites with suitable bandgap, film quality, and optoelectronic properties for front cells is also regarded as one of the limiting factors for improving the performance of TSCs. Because of this problem, many research groups put forward some methods to solve it. For in-

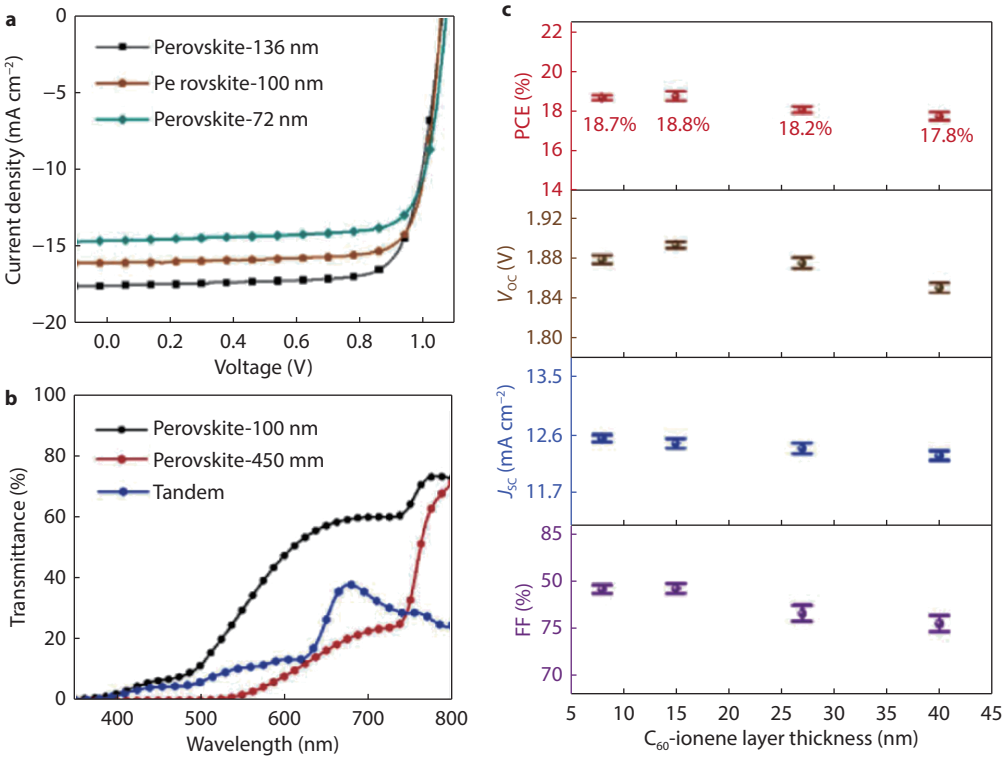

Fig. 8 **a** *J-V* curves of representative PSCs. **b** Transmittance measurement of the perovskite films with different thicknesses and tandem devices. **c** Photovoltaic performance of tandem devices with different thicknesses of C_{60}-ionene films in interconnecting layers (average values with standard deviation were obtained from 15 individual devices; the thicknesses of C_{60}-ionene films were determined by optical profilometry)[97]. Copyright 2022, American Chemical Society.

DOI: 10.54227/elab.20230002

stance, Xie et al. introduced a small amount of formamidinium (FA^+) cations and thiocyanate anions into the basic composition of hybrid perovskite, which provides an effective means to modulate the crystallization properties and phase stability of the films. As shown in Figure 9, the $MA_{0.96}FA_{0.1}PbI_2Br(SCN)_{0.12}$ high-quality films with grain boundaries homogeneously passivated by PbI_2, leading to a reduction in defect states and an enhancement in phase stability. At optimized components, a tandem cell integrated with an organic BHJ (PM6:CH1007) rare cell achieved a PCE of 21.2%[98].

Another core part of 2T monolithic tandem photovoltaics are the interconnecting layers, which play a critical role in modulating the carrier transport and recombination between sub-cells. In the same year, through investigating the change of ICLs composition layer thickness on the ICLs optical and electrical properties, sub-cells EQE properties, and tandem device J-V properties, the relationship between ICLs architecture and 2T monolithic perovskite/organic tandem device performance have been studied by the same group for the first time. They adopted a typical ICL with the architecture of PCBM/BCP/Au/MoO_3 to investigate its role in modulating the carrier transport and recombination between sub-cells. After comparing the thickness of PCBM, BCP and MoO_3 carefully, a conclusion is drawn that the thick ETL will lead to inefficient electron extraction to the ICLs to recombine with the holes extracted from the other side. But by contrast, the carrier modulation ability of ICLs is less sensitive to the MoO_3 film thickness due to its intrinsic high carrier mobility. To sum up, the carrier modulating the ability of the ICLs is strongly associated with the composed ETL thickness and profoundly affect the photoelectric performance of the tandem devices[99]. However, although many strategies have been used to improve the performance of perovskite/organic tandem devices, the PCE of TSCs is still lower than the highest PCE of single PSCs. Considering two sub-cells separately, Qin's group first designed and synthesized a new infrared-absorbing organic small molecule acceptor BTPV-4Cl-eC9 as the narrow bandgap (NBG) organic rear cell and then they introduced an organic cation chloro-formamidinium to passivate the bulk defects in perovskite film. The incorporated $ClFA^+$ successfully passivated the defects and improved the film quality, hence the front perovskite solar cell demonstrated a high PCE of 17.6% with a high V_{oc} of 1.25 V[100]. Synthetic BTPV-4Cl-eC9 with chlorine substituents shows a further red-shifted absorption than the molecule BTPV-4F-eC9. By using PTB7-Th as polymer donor and BTPV-4Cl-eC9 as acceptor, the OSCs achieved an impressive J_{sc} of 28.6 mA cm^{-2}. And the 2T perovskite /organic TSC achieved a high PCE of up to 22.0% with little hysteresis and excellent stability under UV light soaking. Recently, because the short circuit current density of 2T tandem solar cells is limited by sub-cells, many researchers aim to reduce the open-circuit voltage loss of wide-bandgap perovskite sub-cells and select the ideal interconnecting layers of

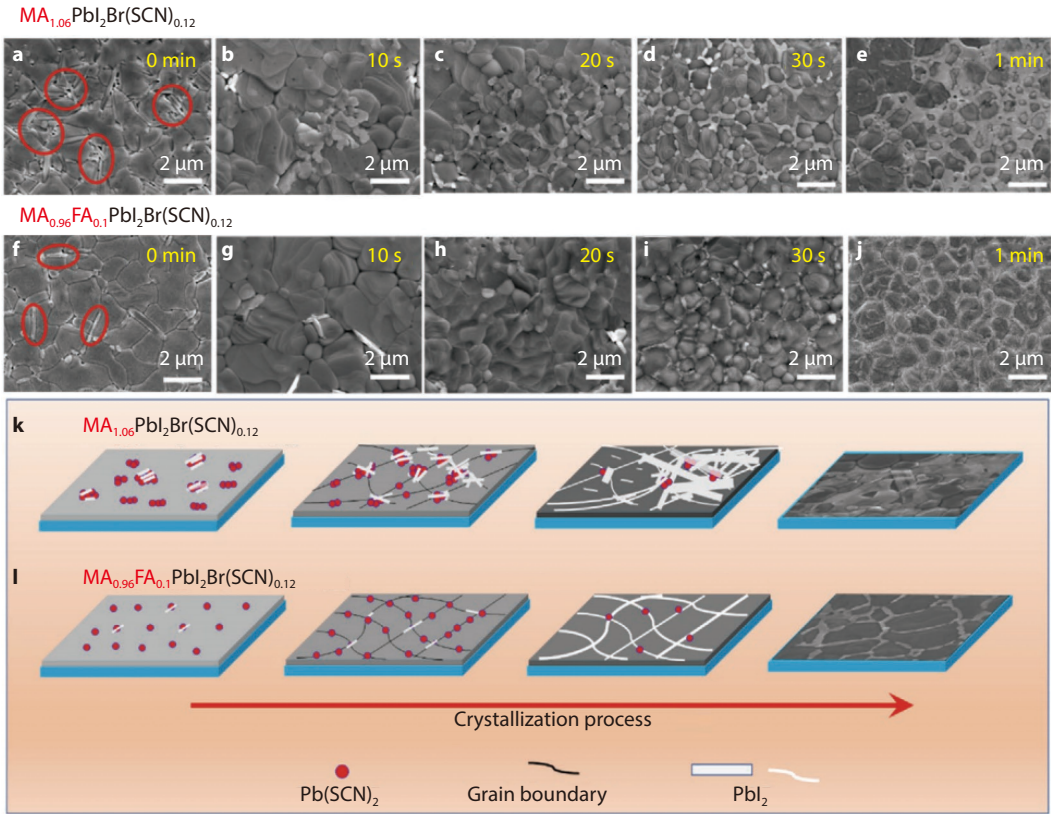

Fig. 9 SEM images of $MA_{1.06}PbI_2Br(SCN)_{0.12}$ films taken with annealing time of **a** 0 s, **b** 10 s, **c** 20 s, **d** 30 s, and **e** 1 min, respectively, and the SEM images of $MA_{0.96}FA_{0.1}PbI_2Br(SCN)_{0.12}$ films taken with annealing time of **f** 0 s, **g** 10 s, **h** 20 s, **i** 30 s, and **j** 1 min, respectively. Schematic illustration of the film formation processes for the **k** $MA_{1.06}PbI_2Br(SCN)_{0.12}$ film and **l** the $MA_{0.96}FA_{0.1}PbI_2Br(SCN)_{0.12}$ film[98]. Copyright 2022, John Wiley and Sons.

DOI: 10.54227/elab.20230002

the tandem devices. In 2022, Chen et al. reported a passivation strategy of nickel oxide hole-transporting layers with benzylphosphonic acid (BPA) leads to prevent interfacial recombination, achieving a high V_{oc} of 1.26 V in a 1.79-eV-bandgap perovskite sub-cell. The introduction of BPA molecules effectively inhibits the non-radiative recombination at the interface and thus more efficient charge collection. The top perovskite sub-cells with a composition of $Cs_{0.25}FA_{0.75}Pb(I_{0.6}Br_{0.4})_3$ got a maximum PCE of 17.80% with a V_{oc} of 1.26 V, a J_{sc} of 17.90 mA cm^{-2} and FF of 78.9%[101]. On the other hand, having demonstrated improved performance of the WBG perovskite sub-cell, they considered the overall design of the perovskite/organic TSC and developed an optimized interconnecting layer structure based on a sputtered indium zinc oxide (IZO) layer. They deposited thin IZO layers with a thickness variation from 2 nm to 6 nm to investigate the impact on the performance of TSCs. Their best small-area tandem device yielded a PCE of 23.60% with optimized 4 nm IZO-based ICLs. The device exhibited a stabilized steady power output of 23.54% and excellent current matching between the two sub-cells, as estimated from the integrated EQE (Figure 10). It is worth mentioning that they also prepared PO-TSCs with a large area of 1.05 cm^2 and achieved a PCE of 21.77%. Using similar perovskite front sub-cell ($FA_{0.8}Cs_{0.2}Pb(I_{0.5}Br_{0.5})_3$) and the same organic back sub-cell (PM6:Y6), Brinkmann et al. obtained a 24% PCE for the 2T TSCs, which is the highest reported value of perovskite/organic tandem devices so far. The sub-cells are connected by an ultrathin (approximately 1.5 nanometers) metal-like indium oxide layer with unprecedentedly low optical/electrical losses. Compared with thin silver, the ultrathin ALD-grown In-O_x layer with a thickness of only about 1.5 nm provides a similarly high carrier density but avoids notable optical losses. Profit from low-loss recombination interconnect and excellent current matching, a champion tandem cell achieved a stabilized PCE of 24.0% and performed excellent stability of more than 1000 h with no sign of degradation when the devices are kept under an inert atmosphere[102]. This work once again reminds us of the importance of the design of efficient interconnection layers for improving the perovskite/organic tandem devices.

PO-TSCs also have unique competitiveness in fabricating high-efficiency flexible photovoltaic devices and attract more and more attention in recent years. Li and co-workers developed efficient perovskite-organic monolithic tandem solar cells by integrating the wide bandgap perovskite (1.74 eV) and low bandgap organic active PBDB-T:SN6IC- 4F (1.30 eV) layer together, which served as the top and bottom sub-cell, respectively[103]. The TSCs based on the PMABr passivated wide-bandgap perovskite sub-cell show a remarkable PCE of 15.13%, with a V_{oc} of 1.85 V, a J_{sc} of 11.52 mA cm^{-2} and FF of 70.98%. After that, taking advantage of the low-temperature solution processability of both perovskite and organic materials, a flexible TSC with a high PCE of 13.61% was realized. Besides, they creatively applied the rigid and flexible PO-TSCs into the solar-to-hydrogen system and generated a solar-to-

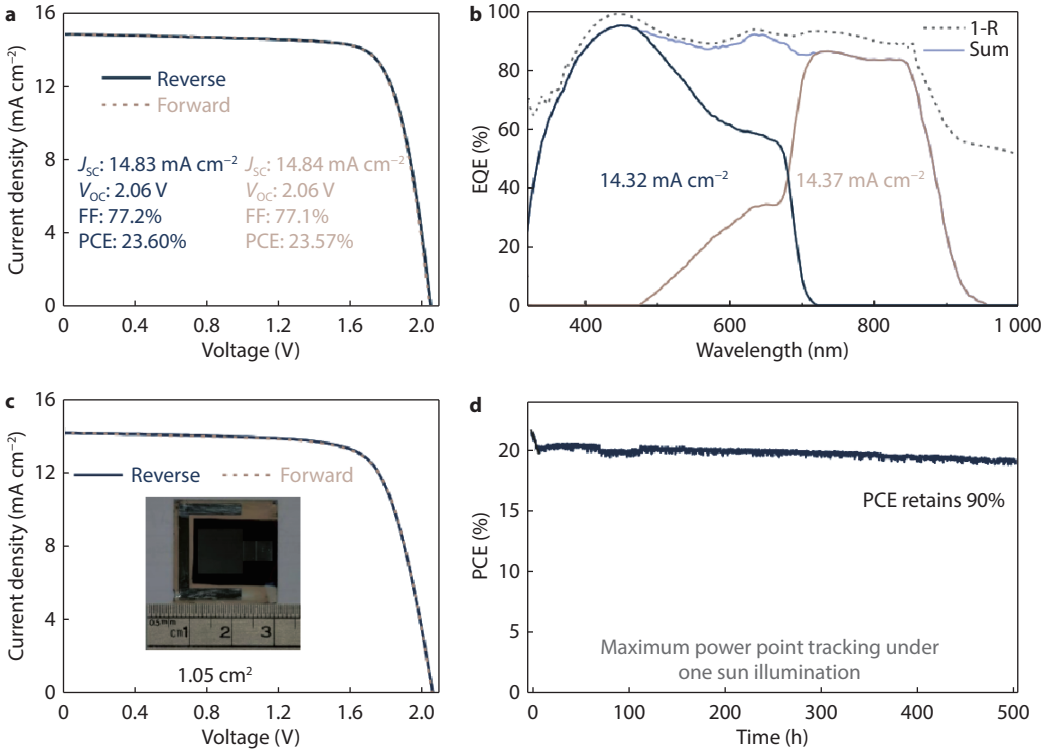

Fig. 10 Optimal performance of the perovskite/organic TSCs. **a** *J-V* curves (reverse and forward scans) of the champion small-area (0.08 cm^2) PO-TSC with IZO-based ICLs. **b** EQE and reflection (denoted as 1-R) spectra for the champion device. **c** *J-V* curves (reverse and forward scans) of the champion large-area perovskite/organic TSC with IZO-based ICLs. **d** Operational stability evaluation of the encapsulated small-area perovskite/organic TSC with IZO-based ICL using the maximum power point tracking method in a N_2 environment and without temperature control[101]. Copyright 2022, Springer Nature.

DOI: 10.54227/elab.20230002

hydrogen efficiency of 12.30% and 11.21% respectively, which explored the advanced application of TSCs. Currently, there are few reports on flexible perovskite/organic tandem devices, and we believe that the main reason is that it is more challenging to prepare high-quality and uniform thin films on flexible substrates such as PET and PEN. The presence of rigid materials like ultra-thin silver in the interconnecting layer can also increase the difficulty of film preparation and greatly reduce the cyclic bendability of flexible devices. Conversely, the high PCE and suppleness of flexible tandem devices also reflects their great application prospects and requires more attention and research.

Summary and outlook

In the past few years, perovskite-based tandem solar cells have been developing rapidly, and PO-TSCs have attracted more attention because of their unique solution processability and achieved a high PCE of over 24% now[102]. The tandem structure efficiently balanced the transmission and thermalization loss, leading to improved device performance. Figure 11a-11c show the energy loss analysis results of the single-junction PSCs, OSCs, and 2T TSCs, and Figure 11d provides converted energy as a function of wavelength for single-junction devices and tandem[86]. As demonstrated, the transmission loss of the perovskite single-junction cell (53.34 mW cm^{-2}) is significantly larger than that of OSC (30.44 mW cm^{-2}), but the tandem architecture holds the same transmission loss with the OSC device while the thermalization loss is significantly suppressed. Referring to the obtained theoretical and experimental results, PO-TSCs feature characteristics of high voltage, broad photo-response, and excellent stability provided by perovskite and organic materials respectively, making it considered to be an effective way to break through the S-Q limit of single junction solar cells. And many strategies, such as selecting different absorption layer types, optimizing the thickness of sub-cells, and introducing high-efficiency intermediate recombination layers, are implemented to ameliorate the performance of the tandem device. Benefiting from the successful employment of various low-bandgap materials with strong absorption in NIR region, the perovskite/organic TSCs exhibited great potential for the improvement of the photoelectric conversion efficiency. However, the highest efficiency of perovskite/organic TSCs is still lower than that of the single-junction PSCs and other types of tandem devices with the combination of perovskite/Si or perovskite/perovskite. One reason not to be ignored is the voltage loss caused by severe charge recombination, especially at multiple interfaces of the tandem devices. At present, most of the perovskite/organic tandem devices can achieve a high $J_{sc.}$ The low charge mobility of organic light-absorbing materials and the energy level mismatch between two sub-cells will bring serious carrier recombination, eventually leading to a lower FF and poor PCE[104].

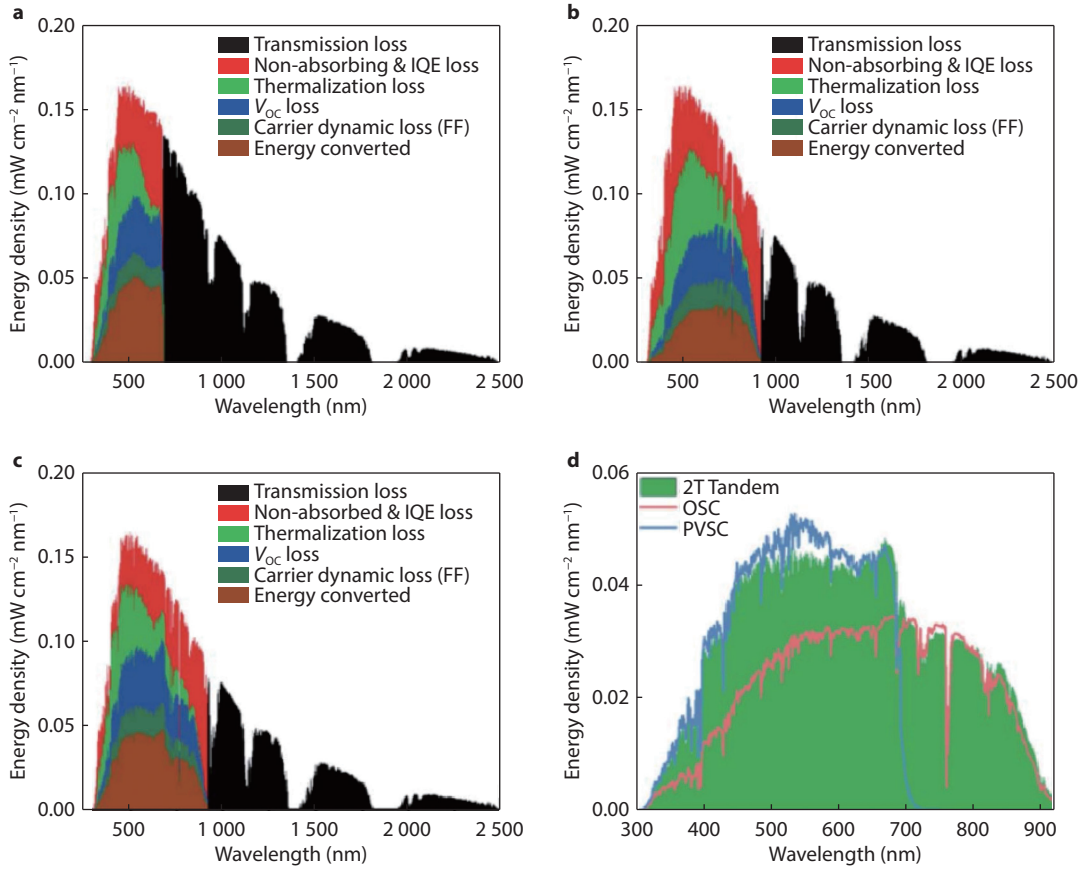

Fig. 11 Calculated energy loss for **a** single-junction PSC, **b** single-junction OSC, and **c** 2T TSC. **d** Converted energy as a function of wavelength for single-junction devices and tandem[86]. Copyright 2021, Royal Society of Chemistry.

DOI: 10.54227/elab.20230002

The unsatisfactory efficiency of PO-TSCs is mainly attributed to the serious V_{oc} loss and carrier dynamic loss caused by the two sub-cells and interconnect layers[86]. In the future development, the charged dynamic and the operational mechanism will need to be more understood and will help to further enhance device photoelectric performance. In addition, the synthesis and application of new materials are also crucial for improving device performance. For example, an ideal organic photovoltaic material PM6:Y6 has been introduced in a tandem architecture to obtain a PCE over 18%, which proves that it is necessary to synthesize new organic photovoltaic materials with stronger near-infrared absorption, higher mobility, and better energy level alignment[105]. Use machine learning, analog computation and collaborations across disciplines to guide material synthesis, improve preparation process, and deeply explore the long-term operation mechanism of devices, etc., to further optimize devices and fully utilize and extract photogenerated carriers.

Although the integration with organic components can improve the stability of the perovskite sub-cell, it still cannot meet the requirements of commercial applications. The stability of PO-TSCs is limited by each sub-cell. It is well known that for perovskite, the most important factor affecting their stability is the water and oxygen in the air, which can accelerate the decomposition of perovskite components. In addition, the phase separation of perovskite components under continuous illumination is also a nonnegligible factor causing poor stability. For OSCs, due to the limitations of organic components, their inherent thermal and chemical stability are not satisfactory, especially the ultraviolet rays in sunlight that are harmful to organic materials. By combining with PSCs to construct a tandem structure, perovskite components can effectively absorb the ultraviolet light portion of the sunlight to protect OPV cells from UV damage. It has been reported that the unencapsulated tandem device is exposed to continuous one-sun illumination in N_2, and after 50 days the PCE retains nearly 90% of its initial value, strongly demonstrating its long-term device stability[90]. According to new research, in a 2T TSC, the UV light could be almost filtered by the front $CsPbI_{1.8}Br_{1.2}$ sub-cell due to its excellent UV stability and filtering effect, thus contributing a robust UV stability to the 2T TSC that enabled it to retain 94.0% of its initial PCE[106]. Recently, Zhu's research team also compared the thermal stability of Cs and FACs based PO-TSC in a glove box nitrogen environment. The results show that, the Cs based devices retained over 85% of its initial PCE after heating at 80 °C for 100 hours while the efficiency of the FACs based devices decreased to less than 50% of its original value after annealing for 100 hours [86]. The stability results suggest that all-inorganic perovskites maybe a better choice to fabricate stable tandem devices with OPV sub-cells.

For practical use, apart from considering high PCE, large-area devices with excellent long-term stability must also take into account and developed. Specifically, the preparation of small module is less economical. However, large-scale preparation of perovskite thin films faces challenges such as non-uniformity and high resistivity, resulting in a significant decrease in PCE. On the premise of not losing its intrinsic characteristics, reducing its horizontal conductivity as much as possible is another crucial issue that must be considered to achieve the scalability of ICL. Manufacturers must systematically redesign and debug material formulations, coating methods, crystallization, lasers, and other aspects to ensure that the efficiency of components under large-scale preparation does not suffer excessive losses. Compared with the individual large-area perovskite or organic solar cells, the combination of the two sub-cells to prepare large-area tandem devices is more conducive to the efficient use of the solar energy spectrum and will greatly reduce the cost of photovoltaic products. If excellent progress can be made, it will be very beneficial to the development of the photovoltaic market in the future[107-112].

Another non-negligible advantage of perovskite/organic tandem structure is the low-temperature solution processability that is suitable for the preparation of high-efficiency flexible devices, but no satisfactory results have been achieved so far. Unlike conventional rigid solar panels, flexible devices can come in various shapes and sizes, and will have more scene applications than conventional solar panels. The main applications are in flexible portable devices, such as solar backpacks, solar tents, and solar flashlights. Compared to perovskite/silicon TSCs, the most significant advantages lie in its flexibility, low cost, and low energy consumption. Therefore, we believe that its application value is mainly reflected in the preparation of flexible devices[113-115]. An important and special application field of flexible perovskite/organic tandem devices is photovoltaic building integration (BIPV), which can be easily and unrestricted integrated on the windows, roofs, and exterior walls of buildings, thereby maximizing the use of solar energy. But there are still many limitations to overcome. It is noted that the currently used ICLs are mainly ultra-thin metal layers and transparent conductive oxides, and their fragility characteristic will restrict the bending stability of flexible devices. In addition, the flexible substrate is not suitable for the deposition method with high temperature, and the flatness of the deposited film will also decline, which is not conducive to the continuous deposition of the underlying film, and is also a potential constraint. If efficient, flexible tandem wearable devices can be successfully prepared, it will also further expand the use of portable photovoltaic products. Hence, TSCs based on large-area or flexible foldable substrates should be researched more for advanced application in the long run.

■ ACKNOWLEDGMENTS

This work is supported by the National Key Research and Development Program of China (2022YFB3803300) and the National Natural Science Foundation of China (51673214). Y.D. also thanks the support from the Fundamental Research Funds for the Central Universities of Central South University (Grant No. 1053320214987).

■ CONFLICT OF INTEREST

The authors declare no conflict of interest.

■ AUTHOR CONTRIBUTIONS

J. Yang directed the overall process. Y. Ding and J. Yang conceived the framework of the review. Y. Ding researched data and wrote the first draft. H. Li, M. Haider, Y. Gao, C. Yi and

DOI: 10.54227/elab.20230002

Z. Zheng revised the manuscript.

REFERENCES

1. K. Yoshikawa, W. Yoshida, T. Irie, H. Kawasaki, K. Konishi, H. Ishibashi, T. Asatani, D. Adachi, M. Kanematsu, H. Uzu, K. Yamamoto, Sol, *Energy Mater. Sol. Cells*, 2017, 173, 37
2. B. Yang, S. Peng, W. C. H. Choy, *EcoMat.*, 2021, 3, e12127
3. F. Qi, X. Deng, X. Wu, L. Huo, Y. Xiao, X. Lu, Z. Zhu, A. K. Y. Jen, *Adv. Energy Mater.*, 2019, 9, 1902600
4. J. Wang, J. Zhang, Y. Zhou, H. Liu, Q. Xue, X. Li, C. C. Chueh, H. L. Yip, Z. Zhu, A. K. Jen, *Nat. Commun.*, 2020, 11, 177
5. R. J. Stoddard, A. Rajagopal, R. L. Palmer, I. L. Braly, A. K. Y. Jen, H. W. Hillhouse, *ACS Energy Lett.*, 2018, 3, 1261
6. Best Research-Cell Efficiency Chart, NREL, https://www.nrel.gov/pv/cell-efficiency.html
7. D. Bi, C. Yi, J. Luo, J. D. Décoppet, F. Zhang, S. M. Zakeeruddin, X. Li, A. Hagfeldt, M. Grätzel, *Nat. Energy*, 2016, 1, 16142
8. N. Jeon, H. Na, E. Jung, T. Y. Yang, Y. G. Lee, G. Kim, H. W. Shin, S. Seok, J. Lee, J. Seo, *Nat. Energy*, 2018, 3, 682
9. X. Luo, X. Lin, F. Gao, Y. Zhao, X. Li, L. Zhan, Z. Qiu, J. Wang, C. Chen, L. Meng, X. Gao, S. (Frank) Liu, R. Zhu, J. Nakazaki, Y. Li, L. Han, *Sci China Chem.*, 2022, 65, 2369
10. S. Li, J. Liu, S. Liu, D. Zhang, C. Liu, D. Li, J. Qi, Y. Hu, A. Mei, H. Han, *EcoMat.*, 2022, 4, e12202
11. J. Jeong, M. Kim, J. Seo, H. Lu, P. Ahlawat, A. Mishra, Y. Yang, M. A. Hope, F. T. Eickemeyer, M. Kim, Y. Yoon, I. Choi, B. P. Darwich, S. J. Choi, Y. Jo, J. H. Lee, B. Walker, S. M. Zakeeruddin, L. Emsley, U. Rothlisberger, A. Hagfeldt, D. S. Kim, M. Grätzel, J. Y. Kim, *Nature*, 2021, 592, 381
12. J. Madan, Shivani, R. Pandey, R. Sharma, *Sol. Energy*, 2020, 197, 212
13. P. Cheng, Y. Liu, S. Y. Chang, T. Li, P. Sun, R. Wang, H.-W. Cheng, T. Huang, L. Meng, S. Nuryyeva, *Joule*, 2019, 3, 432
14. W. Zhao, S. Li, H. Yao, S. Zhang, Y. Zhang, B. Yang, J. Hou, *J. Am. Chem. Soc.*, 2017, 139, 7148
15. Y. Cho, B. Hou, J. Lim, S. Lee, S. Pak, J. Hong, P. Giraud, A. R. Jang, Y. W. Lee, J. Lee, J. E. Jang, H. J. Snaith, S. M. Morris, J. I. Sohn, S. Cha, J. M. Kim, *ACS Energy Lett.*, 2018, 3, 1036
16. P. Wang, Y. Zhao, T. Wang, *Appl. Phys. Rev.*, 2020, 7, 031303
17. N. Lal, Y. Dkhissi, W. Li, Q. Hou, Y. B. Cheng, U. Bach, *Adv. Energy Mater.*, 2017, 7, 1602761
18. G. S. Kinsey, K. M. Edmondson, *Prog. J. Photovolt.*, 2010, 17, 279
19. S. Xing, M. Yun, Z. Chen, A. Kaily, J. Rogers, *Adv. Energy Mater.*, 2015, 5, 1
20. M. Li, J. Fu, Q. Xu, T. Sum, *Adv. Mater.*, 2019, 31, 1802486
21. I. Konovalov, V. Emelianov, *Energy Sci. Eng.*, 2017, 5, 113
22. G. Tang, P. You, Q. Tai, R. Wu, F. Yan, *Sol. RRL*, 2018, 2, 1800066
23. P. Liu, W. Wang, S. Liu, H. Yang, Z. Shao, *Adv. Energy Mater.*, 2019, 9, 1803017
24. Y. Yao, F. Lv, L. Luo, L. Liao, G. Wang, D. Liu, C. Xu, G. Zhou, X. Zhao, Q. Song, *Sol. RRL*, 2020, 4, 1900396
25. P. Holzhey, P. Yadav, S. H. Turren-Cruz, A. Ummadisingu, M. Grätzel, A. Hagfeldt, M. Saliba, *Mater. Today*, 2019, 29, 10
26. Y. C. Shih, L. Wang, H. C. Hsieh, K. J. Lin, *ACS Appl. Mater. Interfaces*, 2018, 10, 11722
27. S. Rahmany, L. Etgar, *ACS Energy Lett.*, 2020, 5, 1519
28. Y. M. Xie, Q. Xue, Q. Yao, S. Xie, T. Niu, H. L. Yip, *Nano Select*, 2021, 1
29. F. Dávid, G. E. Lidón, P. D. R., Daniel, C. Momblona, J. Werner, B. Niesen, C. Ballif, M. Sessolo, H J. Bolink, *Adv. Energy Mater.*, 2017, 7, 1602121
30. H. Fu, W. Gao, Y. Li, F. Lin, X. Wu, J. H. Son, J. Luo, H. Y. Woo, Z. Zhu and A. K. Y. Jen, *Small Methods*, 2020, 4, 2000687
31. T. Todorov, O. Gunawan, S. Guha, *Mol. Syst. Des. Eng.*, 2016, 1, 370
32. J. Di, J. Chang, S. Liu, *EcoMat*, 2020, 2, e12036
33. H. Shen, D. Walter, Y. Wu, K. C. Fong, D. A. Jacobs, T. Duong, J. Peng, K. Weber, T. P. White, K. R. Catchpole, *Adv. Energy Mater.*, 2020, 10, 1902840
34. Q. Jiang, Y. Zhao, X. Zhang, X. Yang, Y. Chen, Z. Chu, Q. Ye, X. Li, Z. Yin and J. You, *Nat. Photonics*, 2019, 13, 460
35. W. Ke, G. Fang, Q. Liu, L. Xiong, P. Qin, H. Tao, J. Wang, H. Lei, B. Li, J. Wan, G. Yang, Y. Yan, *J. Am. Chem. Soc.*, 2015, 137, 6730
36. M. I. Saidaminov, J. Kim, A. Jain, R.Quintero-Bermudez, H. Tan, G. Long, F. Tan, A. Johnston, Y. Zhao, o. Voznyy, E. H. Sargent, *Nature Energy*, 2018, 3, 648
37. X. Li, J. M. Hoffman, M. G. Kanatzidis, *Chem. Rev.*, 2021, 121, 2230
38. K. Xiao, R. Lin, Q. Han, Y. Hou, Z. Qin, H. T. Nguyen, J. Wen, M. Wei, V. Yeddu, M. I. Saidaminov, Y. Gao, X. Luo, Y. Wang, H. Gao, C. Zhang, J. Xu, J. Zhu, E. H. Sargent, H. Tan, *Nat. Energy*, 2020, 5, 870
39. A. F. Palmstrom, G. E. Eperon, T. Leijtens, R. Prasanna, S. N. Habisreutinger, W. Nemeth, E. A. Gaulding, S. P. Duneld, M. Reese, S. Nanayakkara, *Joule*, 2019, 3, 2193
40. C. H. Chiang, C. G. Wu, *Nat. Photonics*, 2016, 10, 196
41. T. Todorov, T. Gershon, O. Gunawan, C. Sturdevant, L. Y. Chang, S. Guha, *Adv. Energy Mater.*, 2015, 5, 1500799
42. A. Rajagopal, Z. Yang, S. B. Jo, L. Braly, P. W. Liang, H. W. Hillhouse, A. K. Y. Jen, *Adv. Mater.*, 2017, 29, 1702140
43. M. Zhang, L. Zhu, T. Hao, G. Zhou, H. H. Huang, *Adv. Mater.*, 2021, 33, 2007177
44. J. Wu, S. C. Liu, Z. Li, S. Wang, D. J. Xue, Y. Lin, J. S. Hu, *National Science Review*, 2021, 8, nwab047
45. S. Wang, W. H. Fang, R. Long, *J. Phys. Chem. Lett.*, 2019, 10, 2445
46. Y. M. Xie, Z. Zeng, X. Xu, C. Ma, Y. Ma, M. Li, C. S. Lee, S. W. Tsang, *Small*, 2020, 16, 1907226
47. L. Dou, C.-C. Chen, K. Yoshimura, K. Ohya, W.-H. Chang, J. Gao, Y. Liu, E. Richard, Y. Yang, *Macromolecules*, 2013, 46, 4734
48. Z. Wang, Z. Song, Y. Yan, S. Liu, D. Yang, *Adv. Sci.*, 2019, 6, 1801704
49. B. Chen, S. W. Baek, Y. Hou, E. Aydin, M. De Bastiani, B. Scheffffel, A. Proppe, Z. Huang, M. Wei, Y.-K. Wang, E. H. Jung, T. G. Allen, E. Van Kerschaver, F. P. Garcı´a De Arquer, M. I. Saidaminov, S. Hoogland, S. De Wolf and E. H. Sargent, *Nat. Commun.*, 2020, 11, 1257
50. Z. Wang, X. Zhu, S. Zuo, M. Chen, C. Zhang, C. Wang, X. Ren, Z. Yang, Z. Liu, X. Xu, Q. Chang, S. Yang, F. Meng, Z. Liu, N. Yuan, J. Ding, S. Liu, D. Yang, *Adv. Funct. Mater.*, 2020, 30, 1908298
51. A. Onno, N. Rodkey, A. Asgharzadeh, S. Manzoor, Z. S. J. Yu, F. Toor, Z. C. Holman, *Joule*, 2020, 4, 580
52. M. T. Ho¨rantner, T. Leijtens, M. E. Zifffffer, G. E. Eperon, M. G. Christoforo, M. D. McGehee, H. J. Snaith, *ACS Energy Lett.*, 2017, 2, 2506
53. Y. Hu, L. Song, Y. Chen, W. Huang, *Sol. RRL*, 2019, 3, 1900080
54. K. Jger, P. Tillmann, E. A. Katz, C. Becker, *Sol. RRL*, 2021, 5, 2000628
55. R. Xue, M. Zhang, D. Luo, W. Chen, R. Zhu, Y. M. Yang, Y. Li, Y. Li, *Sci. China Chem.*, 2020, 63, 987
56. G. Kim, H. Min, K. S. Lee, D. Y. Lee, S. M. Yoon, S. I. Seok, *Science*, 2020, 370, 108
57. J. Hu, Q. Cheng, R. Fan, H. Zhou, *Sol. RRL*, 2017, 1, 1700045
58. X. Chen, Z. Jia, Z. Chen, T. Jiang, L. Bai, F. Tao, J. Chen, X. Chen, T. Liu, X. Xu, C. Yang, W. Shen, W. E. I. Sha, H. Zhu, Y. Yang, *Joule*, 2020, 4, 1594
59. S. Sanchez, N. Christoph, B. Grobety, N. Phung, U. Steiner, M. Saliba, A. Abate, *Adv. Energy Mater.*, 2018, 8, 1802060
60. Y. Cui, H. Yao, B. Gao, Y. Qin, S. Zhang, B. Yang, C. He, B. Xu, J. Hou, *J. Am. Chem. Soc.*, 2017, 139, 7302

DOI: 10.54227/elab.20230002

61. K. M. Yeom, S. U. Kim, M. Y. Woo, J. H. Noh, S. H. Im, *Adv. Mater.*, 2020, 32, 2002228
62. K. Wang, L. Zheng, T. Zhu, X. Yao, C. Yi, X. Zhang, Y. Cao, L. Liu, W. Hu, X. Gong, *Nanomater. Energy*, 2019, 61, 352
63. K. Ghosh, C. Y. Yue, M. M. Sk, R. K. Jena, *ACS Appl. Mater. Interfaces*, 2017, 9, 15350
64. T. Leijtens, K. A. Bush, R. Prasanna, M. D. McGehee, *Nat. Energy*, 2018, 3, 828
65. W. Chen, H. Sun, Q. Hu, A. B. Djurišić, T. P. Russell, X. Guo, Z. He, *ACS Energy Lett.*, 2019, 4, 2535
66. Y. Shen, Y. Liu, H. Ye, Y. Zheng, Q. Wei, Y. Xia, Y. Chen, K. Zhao, W. Huang, S. Liu, *Angew. Chem. Int. Ed.*, 2020, 59, 14896
67. H. Wei, Y. Fang, P. Mulligan, W. Chuirazzi, H. H. Fang, C. Wang, B. R. Ecker, Y. Gao, M. A. Loi, L. Cao, J. Huang, *Nat. Photonics*, 2016, 10, 333
68. Y. Gao, K. Huang, C. Long, Y. Ding, J. Chang, D. Zhang, E. Lioz, M. Liu, J. Yang, *ACS Energy Lett.*, 2022, 7, 1412
69. H. Li, C. Zuo, D. Angmo, H. Weerasinghe, M. Gao, J. Yang, *Nano-Micro Lett.*, 2022, 14, 79
70. Y. Ahmed, B. Khan, M. Bilal Faheem, K. Huang, Y. Gao, J. Yang, *J. Energy Chem.*, 2022, 67, 361
71. C. Long, M. He, K. Huang, Y. Peng, P. He, B. Liu, J. Zhang, J. Yang, *Synthetic Met.*, 2020, 269, 116564
72. H. Li, C. Zuo, A. Scully, D. Angmo, J. Yang, M. Gao, *Flex. Print. Electron.*, 2020, 5, 014006
73. K. Huang, Y. Peng, Y. Gao, J. Shi, H. Li, X. Mo, H. Huang, Y. Gao, L. Ding, J. Yang, *Adv. Energy Mater.*, 2019, 9, 1901419
74. Y. Cui, H. Yao, J. Zhang, K. Xian, T. Zhang, L. Hong, Y. Wang, Y. Xu, K. Ma, C. An, C. He, Z. Wei, F. Gao, J. Hou, *Adv. Mater.*, 2020, 32, 1908205
75. D. H. Kim, J. H. Heo, S. H. Im, *ACS Appl. Mater. Interfaces*, 2019, 11, 19123
76. G. E. Eperon, T. Leijtens, K. A. Bush, R. Prasanna, T. Green, J. T. W. Wang, M. B. Johnston, M. D. McGehee, H. J. Snaith, *Science*, 2016, 354, 861
77. D. Zhao, C. Chen, C. Wang, M. M. Junda, Z. Song, C. R. Grice, Y. Yu, C. Li, B. Subedi, N. J. Podraza, X. Zhao, G. Fang, R. G. Xiong, K. Zhu, Y. Yan, *Nat. Energy*, 2018, 3, 1093
78. B. A. Nejand, I. M. Hossain, M. Jakoby, S. Moghadamzadeh, T. Abzieher, S. Gharibzadeh, J. A. Schwenzer, P. Nazari, F. Schackmar, D. Hauschild, L. Weinhardt, U. Lemmer, B. S. Richards, I. A. Howard, U. W. Paetzold, *Adv. Energy Mater.*, 2020, 10, 1902583
79. Z. Yu, Z. Yang, Z. Ni, Y. Shao, B. Chen, Y. Lin, H. Wei, Z. J. Yu, Z. Holman, J. Huang, *Nat. Energy*, 2020, 5, 657
80. R. Lin, J. Xu, M. Wei, Y. Wang, Z. Qin, Z. Liu, J. Wu, K. Xiao, B. Chen, S. Park, G. Chen, H. R. Atapattu, K. R. Graham, J. Xu, J. Zhu, L. Li, C. Zhang, E. H. Sargent, H. Tan, *Nature*, 2022, 603, 73
81. C. M. Wolff, P. Caprioglio, M. Stolterfoht, D. Neher, *Adv. Mater.*, 2019, 31, 1902762
82. Z. Zheng, J. Wang, P. Bi, J. Ren, Y. Wang, Y. Yang, X. Liu, S. Zhang, J. Hou, *Joule*, 2021, 6, 171
83. L. Arunagiri, Z. Peng, X. Zou, H. Yu, G. Zhang, Z. Wang, J. Y. Lin Lai, J. Zhang, Y. Zheng, C. Cui, F. Huang, Y. Zou, K. S. Wong, P. C. Y. Chow, H. Ade, H. Yan, *Joule*, 2020, 4, 1790
84. K. Lang, Q. Guo, Z. He, Y. Bai, J. Yao, M. Wakeel, M. S. Alhodaly, Z. Tan, *J. Phys. Chem. Lett.*, 2020, 11, 9596
85. H. Aqoma, I. F. Imran, F. T. A. Wibowo, N. V. Krishna, Lee, W. A. K. Sarker, D. Y. Ryu, S. Y. Jang, *Adv. Energy Mater.*, 2020, 10, 2001188
86. X. Wu, Y. Liu, F. Qi, F. Lin, H. Fu, K. Jiang, S. Wu, L. Bi, D. Wang, F. Xu, Alex K. Y. Jen and Z. Zhu, *J. Mater. Chem. A*, 2021, 9, 19778
87. Y. Ding, Q. Guo, Y. Geng, Z. Dai, Z. Wang, Z. Chen, Q. Guo, Z. Zheng, Y. Li, E. Zhou, *Nano Today*, 2022, 46, 101586
88. J. Liu, S. Lu, L. Zhu, X. Li, W C. H. Choy, *Nanoscale*, 2016, 8, 3638
89. L. Liu, H. Xiao, K. Jin, Z. Xiao, X. Du, K. Yan, F. Hao, Q. Bao, C. Yi, F. Liu, W. Wang, C. Zuo, L. Ding, *Nano-Micro Lett.*, 2023, 15, 23
90. Q. Sun, X. Xu, Q. Sun, Q. Yao, Y. Cai, Y. Li, L. Xu, W. He, M. Zhu, X. Lv, R. Lin, A. K. Y. Jen, T. Shi, H. Yip, M. Fung, Y. Xie, *Adv. Energy Mater.*, 2023, 13, 2204347
91. C. Chen, S. H. Bae, W. H. Chang, Z. Hong, G. Li, Q. Chen, H. Zhou and Y. Yang, *Mater. Horiz.*, 2015, 2, 203
92. Y. Liu, L. A. Renna, M. Bag, A. Page, Y. Kim, J. Choi, T. Emrick, D. Venkataraman, P. Russell, *ACS Appl. Mater. Interfaces*, 2016, 8, 7070
93. W. Chen, J. Zhang, G. Xu, R. Xue, Y. Li, Y. Zhou, J. Hou, and Y. Li, *Adv. Mater.*, 2018, 30, 1800855
94. R. Lin, K. Xiao, Z. Qin, Q. Han, C. Zhang, M. Wei, M. I. Saidaminov, Y. Gao, J. Xu, M. Xiao, A. Li, J. Zhu, E. H. Sargent, H. Tan, *Nat. Energy*, 2019, 4, 864
95. X. Chen, Z. Jia, Z. Chen, Wei E. I. Sha, H. Zhu, Y. Yang, *Joule*, 2020, 4, 1
96. L. Zuo, X. Shi, S. B. Jo, Y. Liu, F. Lin, A. K. Y. Jen, *Adv. Mater.*, 2018, 30, 1706816
97. Z. Zhang, C. Cueto, Y. Ding, L. Yu, T. P. Russell, T. Emrick, Y. Liu, *ACS Appl. Mater. Interfaces*, 2022, 14, 29896
98. Y. M. Xie, Q. Yao, Z. Zeng, Q. Xue, T. Niu, R. Xia, Y. Cheng, F. Lin, S. W. Tsang, Alex K. Y. Jen, H. L. Yip, Y. Cao, *Adv. Funct. Mater.*, 2022, 32, 2112126
99. Y. M. Xie, T. Niu, Q. Yao, Q. Xue, Z. Zeng, Y. Cheng, H. L. Yip, Y. Cao, *J. Energy Chem.*, 2022, 71, 12
100. S. Qin, C. Lu, Z. Jia, Y. Wang, S. Li, W. Lai, P. Shi, R. Wang, C. Zhu, J. Du, J. Zhang, L. Meng, Y. Li, *Adv. Mater.*, 2022, 34, 2108829
101. W. Chen, Y. Zhu, J. Xiu, G. Chen, H. Liang, S. Liu, H. Xue, E. Birgersson, J. Ho, X. Qin, J. Lin, R. Ma, T. Liu, Y. He, A. M. C. Ng, X. Guo, Z. He, H. Yan, A. B. Djurišić, Y. Hou, *Nat. Energy*, 2022, 7, 229
102. K. O. Brinkmann, T. Becker, F. Zimmermann, C. Kreusel, T. Gahlmann, M. Theisen, T. Haeger, S. Olthof, C. Tückmantel, M. Günster, T. Maschwitz, F. Göbelsmann, C. Koch, D. Hertel, P. Caprioglio, F. Peña-Camargo, L. Perdigón Toro, A. Al Ashouri, L. Merten, A. Hinderhofer, L. Gomell, S. Zhang, F. Schreiber, S. Albrecht, T. Riedl, *Nature*, 2022, 604, 280
103. X. Luo, T. Wu, Y. Wang, X. Lin, H. Su, Q. Han, L. Han, *Sci. China Chem.*, 2021, 2, 218
104. C. Yan, J. Huang, D. Li, G. Li, *Mater. Chem. Front.*, 2021, 5, 4538
105. K. Jiang, Q. Wei, J. Y. L. Lai, H. Ade, Y. Zou, H. Yan, *Joule*, 2019, 3, 3020
106. W. Chen, D. Li, X. Chen, H. Chen, S. Liu, H. Yang, X. Li, Y. Shen, X. Ou, Y. Yang, L. Jiang, Y. Li, Y. Li, *Adv. Funct. Mater.*, 2022, 32, 2109321
107. S. Xie, R. Xia, Z. Chen, J. Tian, L. Yan, M. Ren, Z. Li, G. Zhang, Q. Xue, H. L. Yip, Y. Cao, *Nano Energy*, 2020, 78, 105238
108. S. Roland, S. Neubert, S. Albrecht, B. Stannowski, M. Seger, A. Facchetti, R. Schlatmann, B. Rech, D. Neher, *Adv. Mater.*, 2015, 27, 1262
109. S. Li, L. Ye, W. Zhao, S. Zhang, S. Mukherjee, H. Ade, J. Hou, *Adv. Mater.*, 2016, 28, 9423
110. W. Zhao, D. Qian, S. Zhang, S. Li, O. Inganäs, F. Gao, J. Hou, *Adv. Mater.*, 2016, 28, 4734
111. Y. Lin, F. Zhao, S. K. K. Prasad, J.-D. Chen, W. Cai, Q. Zhang, K. Chen, Y. Wu, W. Ma, F. Gao, *Adv. Mater.*, 2018, 30, 1706363
112. J. Yuan, Y. Zhang, L. Zhou, G. Zhang, H.-L. Yip, T.-K. Lau, X. Lu, C. Zhu, H. Peng, P. A. Johnson, *Joule*, 2019, 3, 1140
113. Q. An, J. Wang, X. Ma, J. Gao, Z. Hu, B. Liu, H. Sun, X. Guo, X. Zhang, F. Zhang, *Energy Environ. Sci.*, 2020, 13, 5039
114. G. Chai, Y. Chang, J. Zhang, X. Xu, L. Yu, X. Zou, X. Li, Y. Chen, S. Luo, B. Liu, *Energy Environ. Sci.*, 2021, 14, 3469
115. W. Gao, F. Qi, Z. Peng, F. R. Lin, K. Jiang, C. Zhong, W. Kaminsky, Z. Guan, C.-S. Lee, T. J. Marks, H. Ade, A. K.-Y. Jen, *Adv. Mater.*, 2022, 34, 2202089

DOI: 10.54227/elab.20230002

Biographies

Yang Ding majored in condensed matter physics at the School of Physics and Electronics, Central South University (Changsha, China). He received his master's degree from Ocean University of China (Qingdao, China). His research focuses on high-performance perovskite solar cells.

Junliang Yang received his Ph.D. in 2008 from the Changchun Institute of Applied Chemistry, Chinese Academy of Sciences. He then joined Prof. Tim S. Jones' group at the University of Warwick. In 2011, he moved to Australia and joined Prof. Andrew B. Holmes' group at the University of Melbourne and at the Commonwealth Scientific and Industrial Research Organization. In 2012, he was appointed as a professor in the School of Physics and Electronics at Central South University. His research focuses on flexible and printed electronics, organic, and perovskite solar cells.